Nano Research

Maskless micro/nanopatterning and bipolar electrical-rectification of MoS2 flakes through femtosecond laser direct writing

--Manuscript Draft--

Manuscript Number:	
Full Title:	Maskless micro/nanopatterning and bipolar electrical-rectification of MoS2 flakes through femtosecond laser direct writing
Article Type:	Regular Article
Corresponding Author:	Xin Li Beijing Institute of Technology CHINA
Corresponding Author Secondary Information:	
Corresponding Author's Institution:	Beijing Institute of Technology
Corresponding Author's Secondary Institution:	
First Author:	Pei Zuo
First Author Secondary Information:	
Order of Authors:	Pei Zuo
	Lan Jiang
	Xin Li
	Mengyao Tian
	Chenyang Xu
	Yongjiu Yuan
	Peng Ran
	Bo Li
	Yongfeng Lu
Order of Authors Secondary Information:	

| Abstract: | MoS2 micro/nanostructures are desirable for tuning electronic properties, developing required functionality, and improving existing performance of multilayer MoS2 devices. This work presents a useful method to flexibly microprocess multilayer MoS2 flakes through femtosecond laser pulse direct writing, which can directly fabricate regular MoS2 nanoribbon arrays with ribbon widths of 179, 152, 116, 98, and 77 nm, and arbitrarily pattern MoS2 flakes to form micro/nanostructures such as single nanoribbon, labyrinth array, and cross structure. This method is mask-free and simple, and has high flexibility, strong controllability, and high precision. Moreover, numerous oxygen molecules are chemically and physically bonded to laser-processed MoS2, attributed to roughness defect-sites and edges of micro/nanostructures that contain numerous unsaturated edge-sites and highly active centres. In addition, electrical tests of the field effect transistor fabricated from prepared MoS2 nanoribbon arrays reveal new interesting features: output and transfer characteristics exhibit strong rectification (not |

	going through zero and bipolar conduction) of drain−source current, which is supposedly attributed to the coordinate structures and p-type chemical doping of oxygen molecules on MoS2 nanoribbon arrays. This work demonstrates the ability of femtosecond laser pulses to directly induce micro/nanostructures, property changes, and new device-properties of two-dimension materials, which may future enable new device applications.
Suggested Reviewers:	Minlin Zhong Tsinghua University zhml@tsinghua.edu.cn
	Minghui Hong National University of Singapore elehmh@nus.edu.sg
	Zheyu Fang Peking University zhyfang@pku.edu.cn
	E. Stratakis University of Crete stratak@iesl.forth.gr
	Xiaogan Liang University of Michigan xiaoganl@umich.edu

Xin Li, Professor
Laser Micro/Nano Fabrication Laboratory
School of Mechanical Engineering
Beijing Institute of Technology
Beijing, 100081, China
Phone: 86-10-68914524；Email: lixin02@bit.edu.cn

Dear Editor,

We would like to submit enclosed manuscript entitled "Maskless micro/nanopatterning and bipolar electrical-rectification of MoS_2 flakes through femtosecond laser direct writing", which we wish to be considered for publication in "*Nano Research*". No conflict of interest exits in the submission of this manuscript, and manuscript is approved by all authors for publication. I would like to declare on behalf of my co-authors that the work described is original research that has not been published previously, and not under consideration for publication elsewhere, in whole or in part. All the authors listed have approved the manuscript that is enclosed.

Molybdenum disulfide (MoS_2) is a typical member of the transition metal dichalcogenides family, a kind of graphene-like two-dimensional materials which are one of the most popular materials recently. MoS_2 micro/nanostructures are desirable for tuning electronic properties, developing required functionality, or improving existing performance of MoS_2 devices. Hence, it is crucial to conduct research on MoS_2 patterning with ordered micro/nanostructures, controlled structure-size, and device application having new features.

This work presents a useful method to flexibly microprocess multilayer MoS_2 flakes through femtosecond laser pulse direct writing, which can directly fabricate regular MoS_2 nanoribbon arrays with ribbon widths of 179, 152, 116, 98, and 77 nm, and arbitrarily pattern MoS_2 flakes to form micro/nanostructures such as single nanoribbon, labyrinth array, and cross structure. This method is mask-free and simple, and has high flexibility, strong controllability, and high precision. Moreover, numerous oxygen molecules are chemically and physically bonded to laser-processed MoS_2, attributed to roughness defect-sites and edges of micro/nanostructures that contain numerous unsaturated edge-sites and highly active centres. In addition, electrical tests of the field effect transistor fabricated from prepared MoS_2 nanoribbon arrays reveal new interesting features: output and transfer characteristics exhibit strong rectification (not going through zero and bipolar conduction) of drain−source current, which is supposedly attributed to the coordinate structures and p-type chemical doping of oxygen molecules on MoS_2 nanoribbon arrays. This work

demonstrates the ability of femtosecond laser pulses to directly induce micro/nanostructures, property changes, and new device-properties of two-dimension materials, which may future enable new device applications.

We deeply appreciate your consideration of our manuscript, and we look forward to receiving comments from the reviewers. If you have any queries, please don't hesitate to contact me at lixin02@bit.edu.cn.

Thank you and best regards,

Yours sincerely,

Xin Li, Professor
Beijing Institute of Technology

Template for Preparation of Manuscripts for *Nano Research*

This template is to be used for preparing manuscripts for submission to *Nano Research*. Use of this template will save time in the review and production processes and will expedite publication. However, use of the template is not a requirement of submission. Do not modify the template in any way (delete spaces, modify font size/line height, etc.). If you need more detailed information about the preparation and submission of a manuscript to *Nano Research*, please see the latest version of the Instructions for Authors at http://www.thenanoresearch.com/.

TABLE OF CONTENTS (TOC)

Authors are required to submit a graphic entry for the Table of Contents (TOC) in conjunction with the manuscript title. This graphic should capture the readers' attention and give readers a visual impression of the essence of the paper. Labels, formulae, or numbers within the graphic must be legible at publication size. Tables or spectra are not acceptable. Color graphics are highly encouraged. The resolution of the figure should be at least 600 dpi. The size should be at least 50 mm × 80 mm with a rectangular shape (ideally, the ratio of height to width should be less than 1 and larger than 5/8). One to two sentences should be written below the figure to summarize the paper. To create the TOC, please insert your image in the template box below. Fonts, size, and spaces should not be changed.

Maskless micro/nanopatterning and bipolar electrical-rectification of MoS$_2$ flakes through femtosecond laser direct writing

Pei Zuo[1], Lan Jiang[1], Xin Li[1,*], Mengyao Tian[1], Chenyang Xu[1], Yongjiu Yuan[1], Peng Ran[1], Bo Li[1], Yongfeng Lu[2]

1 Beijing Institute of Technology, China

2 University of Nebraska-Lincoln, USA
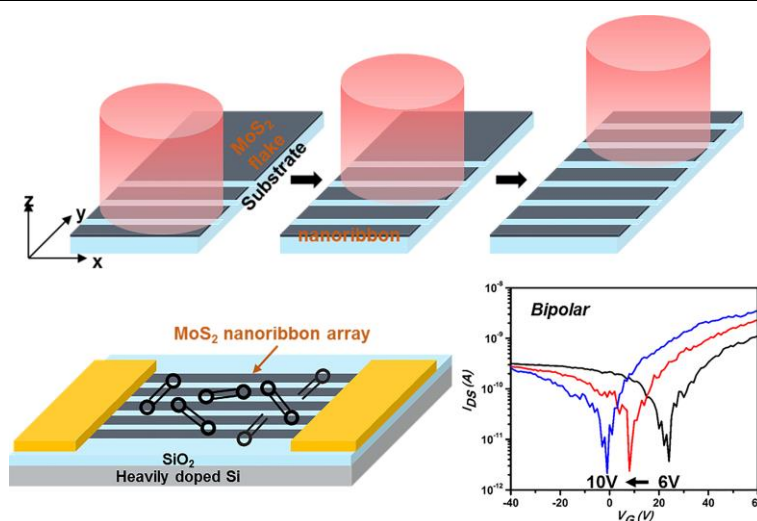
This work presents a useful method to microprocess multilayer MoS$_2$ flakes through femtosecond laser pulse direct writing, which can directly fabricate regular MoS$_2$ nanoribbon arrays with different ribbon widths and arbitrarily pattern MoS$_2$ flakes to form micro/nanostructures. Electrical tests of field effect transistor fabricated from prepared MoS$_2$ nanoribbon arrays reveal new interesting features: output and transfer characteristics exhibit strong rectification (not going through zero and bipolar conduction) of drain−source current.

1
2
3
4
5
6
7
8
9
10
11
12
13
14
15
16
17
18
19
20
21
22
23
24
25
26
27
28
29
30
31
32
33
34
35
36
37
38
39
40
41
42
43
44
45
46
47
48
49
50
51
52
53
54
55
56
57
58
59
60
61
62
63
64
65

Maskless micro/nanopatterning and bipolar electrical-rectification of MoS₂ flakes through femtosecond laser direct writing

Pei Zuo[1], Lan Jiang[1], Xin Li[1] (✉), Mengyao Tian[1], Chenyang Xu[1], Yongjiu Yuan[1], Peng Ran[1], Bo Li[1], Yongfeng Lu[2]

[1] *Laser Micro/Nano Fabrication Lab, School of Mechanical Engineering, Beijing Institute of Technology, Beijing 100081, China*
[2] *Laser Assisted Nano Engineering Lab, Department of Electrical Engineering, University of Nebraska-Lincoln, Lincoln, NE 68588-0511, USA*

ABSTRACT

MoS₂ micro/nanostructures are desirable for tuning electronic properties, developing required functionality, and improving existing performance of multilayer MoS₂ devices. This work presents a useful method to flexibly microprocess multilayer MoS₂ flakes through femtosecond laser pulse direct writing, which can directly fabricate regular MoS₂ nanoribbon arrays with ribbon widths of 179, 152, 116, 98, and 77 nm, and arbitrarily pattern MoS₂ flakes to form micro/nanostructures such as single nanoribbon, labyrinth array, and cross structure. This method is mask-free and simple, and has high flexibility, strong controllability, and high precision. Moreover, numerous oxygen molecules are chemically and physically bonded to laser-processed MoS₂, attributed to roughness defect-sites and edges of micro/nanostructures that contain numerous unsaturated edge-sites and highly active centres. In addition, electrical tests of the field effect transistor fabricated from prepared MoS₂ nanoribbon arrays reveal new interesting features: output and transfer characteristics exhibit strong rectification (not going through zero and bipolar conduction) of drain−source current, which is supposedly attributed to the coordinate structures and p-type chemical doping of oxygen molecules on MoS₂ nanoribbon arrays. This work demonstrates the ability of femtosecond laser pulses to directly induce micro/nanostructures, property changes, and new device-properties of two-dimension materials, which may future enable new device applications.

KEYWORDS

MoS₂ flakes, femtosecond laser direct writing, micro/nanopatterning, oxygen bonding, electrical rectification

1 Introduction

Transition metal dichalcogenides (TMDCs), representative layered materials like graphene, have been widely studied as a family of new-type semiconducting materials with extraordinary mechanical, electrical, and optical properties, and great promise for extensive applications [1-6]. Molybdenum disulfide (MoS₂), representative material belonging to the TMDC group, has lattice structure of a layer of molybdenum atoms sandwiched between two layers of sulfur atoms [7, 8]. Unlike graphene with zero-band-gap, MoS₂ is a band-gap semiconductor with sizable energy band gap [5, 9]: MoS₂ in bulk form has indirect energy gap of ~1.2 eV and MoS₂ in monolayer form has direct band gap of ~1.8 eV [3]. Hence, MoS₂ can serve as a promising candidate of graphene, and has excellent potential in semiconductor-related applications of layered materials such as thin-film transistors [1, 10], integrated circuits [11, 12], complementary inverter [13], photodetectors [14], light-emitting diodes [15, 16], photovoltaics [17, 18], superconductors [19, 20], and chemical/biological sensors [21, 22].

To achieve desirable electronic properties and required functionality and improve existing performance of MoS₂ devices, a microfabrication process is usually required to fabricate large arrays of orderly arranged MoS₂ micro/nanostructures, commonly involving patterning and etching [3, 23]. Hence, it is crucial to

conduct research on MoS₂ patterning with ordered micro/nanostructures, controlled structure-size, and device application having new features. Several approaches have been attempted to pattern MoS₂ materials or fabricate micro/nanostructures of MoS₂ deposited on substrates, including tape exfoliation [24, 25], chemical vapor deposition (CVD) [26, 27], thermal decomposition of thiosalts [28], van der Waals epitaxial growth [29, 30], patterned MoO3 sulfurization [31, 32], CVD in plasma-treated areas [33, 34], block copolymer lithography [35], reactive ion etching (RIE) combined with deposition in plasma-treated areas [3], lithography combined with stamping [23], lithography combined with RIE [36, 37], and continue wave (CW) laser direct processing [38, 39]. Among them, CVD in plasma-treated areas, block copolymer lithography, lithography combined with deposition in plasma-treated areas, lithography combined with stamping, lithography combined with RIE, and CW laser direct processing can realize control for the location, shape, and size of MoS₂ micro/nanostructures. Whereas, in the methods involving lithography, plasma surface treatment, and RIE, chemical organics (such as photoresist) and inorganic or organic masks are used, combined process are required, and the integral process is relatively complex. CW laser direct processing is a one-step process and is simple, no special atmosphere system and mask are needed, cost is relatively low, and flexibility and controllability are high. Whereas, CW laser processing is a thermal

Address correspondence to Xin Li, lixin02@bit.edu.cn

process, and the strong thermal effect would cause thermal oxidization of materials and lead to large recasting layer, hence processing precision is insufficient. Femtosecond (ultrafast) laser pulse direct processing is another kind of laser processing technology. Femtosecond laser pulses have ultrashort pulse width, ultrahigh power density, and nonlinear nonequilibrium processing feature, and multiphoton absorption and nonthermal effect can be realized, hence except including almost all the advantages of CW laser processing, femtosecond laser direct processing also possesses high processing precision [40].

In this work, we proposed a useful method of utilizing femtosecond laser pulse direct writing to modify multilayer MoS_2 flakes, directly fabricate regular MoS_2 nanoribbon arrays with different ribbon widths, and arbitrarily pattern MoS_2 flakes to form different MoS_2 micro/nanostructures. Moreover, the laser-fabricated MoS_2 structures were chemically and physically bonded with numerous oxygen molecules in the air, which can be attributed to the roughness defect-sites and long edges of the nanoribbons that may contain numerous unsaturated edge sites and highly active centres. At last, electronic properties of MoS_2 nanoribbon arrays fabricated to be field effect transistor (FET) were tested, and the output and transfer characteristics exhibited strong rectification (not went through zero and exhibited bipolar conduction) of drain−source current. This rectification was supposedly attributed to the coordinate structures and p-type chemical doping of oxygen molecules on MoS_2 nanoribbon arrays, which may cause transition of n-type channel to p-type channel or properties similar to pn junction. The proposed method had advantages of simplicity, maskless, strong controllability, high flexibility, and high precision, and also indicated the ability of femtosecond laser pulses to directly induce two-dimension micro/nanostructures/patterns, property changes of two-dimension material, and new device features.

2 Results and discussion

In this work, multilayer MoS_2 flakes were mechanically exfoliated from a natural crystal and deposited on 300nm-SiO_2/Si substrates. The thickness of MoS_2 flakes selected for experiments was several to dozens of nanometers. The schematic of our method of fabricating MoS_2 nanoribbons/patterns is shown in Fig. 1a, which relies on the formation of regular nanostructures and the material removal by femtosecond laser pulse irradiation. When femtosecond laser pulse beam is focused and irradiated on material surface, surface plasmons (SPs) can be induced on the material surface, interference of which with incident laser field can lead to the formation of initial grating structures on material, then these initial grating structures can assist the coupling of SPs and incident laser field, leading to the further formation of final grating structures with deeper gaps [41]. The depth of gaps of laser induced grating structures is influenced by the number and energy of ultrafast laser pulses on unit area of material, and can be on a micrometer scale [40, 42, 43]. The MoS_2 used in our experiment was nano-scale thin flake, therefore controlling scan speed of laser beam enough slow (laser pulse number on unit area of MoS_2 enough large) can control the gaps penetrating the whole MoS_2 thin flake, enabling surface nanogratings to become independent nanoribbons. Figure 1b shows the optical comparison of pristine MoS_2 with femtosecond laser-processed (FLP-) MoS_2, which showed obviously optical color change of MoS_2 flake after femtosecond laser irradiation, indicating the change in thickness or surface roughness. Figure 1c shows the atomic force microscope (AFM) results of MoS_2 flake in Fig. 1b, which indicates a reduction of outline height of FLP-MoS_2 flake, suggesting the thinning effect on MoS_2 by femtosecond laser irradiation. Figure 1d shows the high resolution AFM image of FLP-MoS_2, which indicated the formation of MoS_2 grating structures.
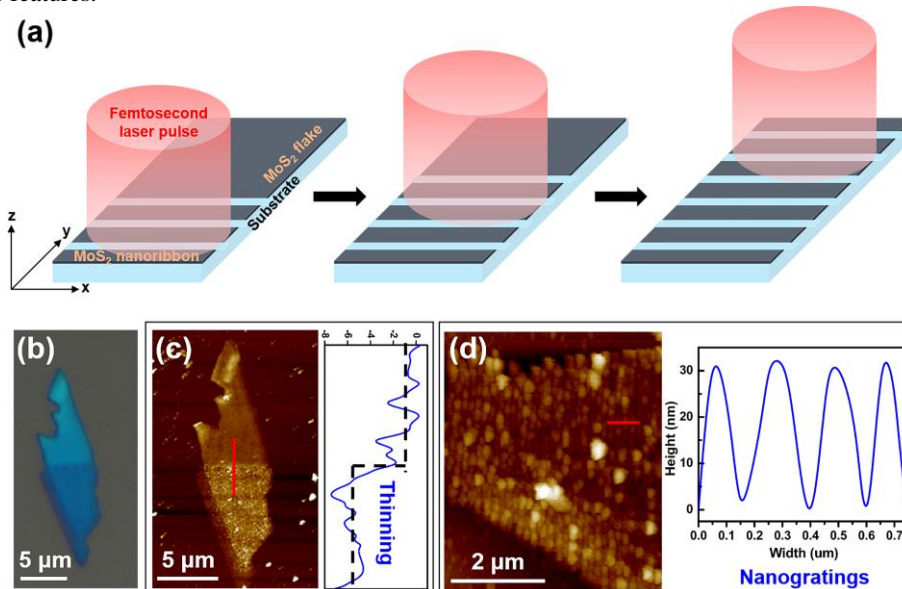

Figure 1 Principle and preliminary characterization of this method. (a) Schematic of femtosecond laser direct wiring processing to induce MoS_2 nanoribbons array. (b) Optical comparison of pristine MoS_2 (upper part) with FLP-MoS_2 (lower part). (c) AFM and (d) high resolution AFM of the FLP-MoS_2 flake.

To further investigate the FLP-MoS_2 micro/nanostructures, scanning electron microscope (SEM) was carried out to characterize its physical morphology, as shown in Fig. 2. Figure 2a-e show regular MoS_2 nanoribbon arrays with different ribbon widths of approximate 179, 152, 116, 98, and 77 nm, respectively. Figure 2f shows two independent MoS_2 nanoribbons with small and big width of 56 and 420 nm, respectively. Figure 2g and h show two kind of MoS_2 patterned structures obtained through material removal by femtosecond laser direct writing, which were a labyrinth array and a cross structure, indicating the flexible processing capability of femtosecond laser for arbitrary patterns.
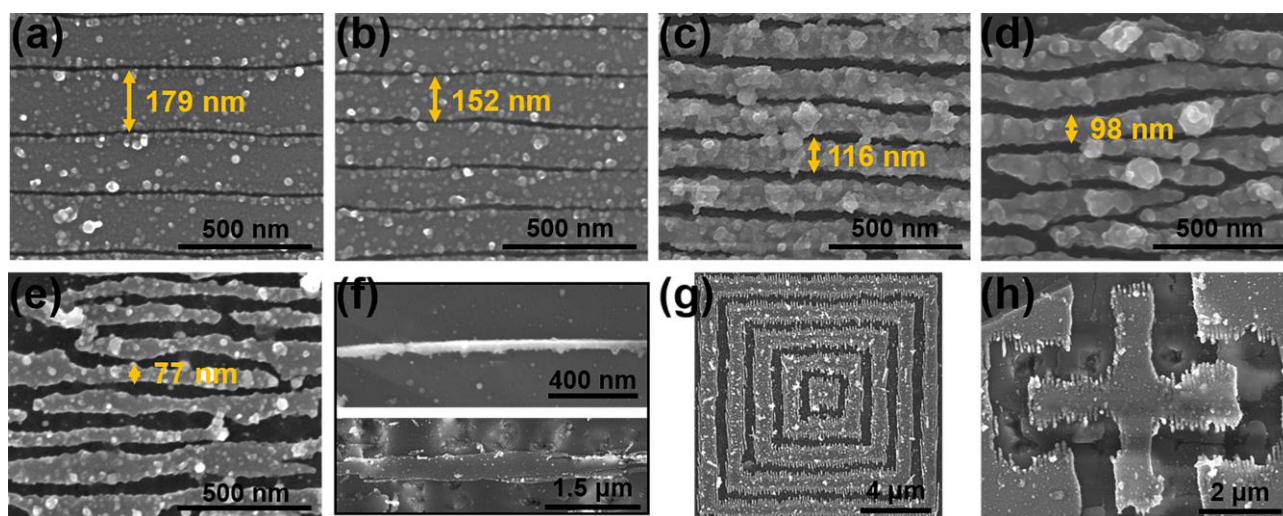
Figure 2 FLP-MoS$_2$ micro/nanostructures and patterns. (a-e) SEM images of regular MoS$_2$ nanoribbon arrays with widths of 179, 152, 116, 98, and 77 nm, respectively. (f) SEM images of two independent MoS$_2$ nanoribbons with width of (up) 56 and (down) 420 nm. SEM images of (g) MoS$_2$ labyrinth array and (h) MoS$_2$ cross structure.

To investigate the formation of MoS$_2$ nanoribbons rather than surface structures on MoS$_2$, energy dispersive X-ray (EDX) analysis was performed. Figure 3a-c show the SEM images of the edge of a FLP-MoS$_2$ flake, and its S and Si EDX mapping images. The grey part denotes MoS$_2$, the black part denotes substrate, and the regular stripe structures were obtained through the irradiation of femtosecond laser pulses (Fig. 3a). Figure 3b shows the clearly separated MoS$_2$ nanoribbons, and Fig. 3c shows the clear gaps between these MoS$_2$ nanoribbons. Figure 3d-f shows the SEM image of MoS$_2$ nanoribbon arrays, and their S and Si EDX mapping images, which also indicated the separation of MoS$_2$ nanoribbons, thus evidencing the formation of MoS$_2$ nanoribbons.
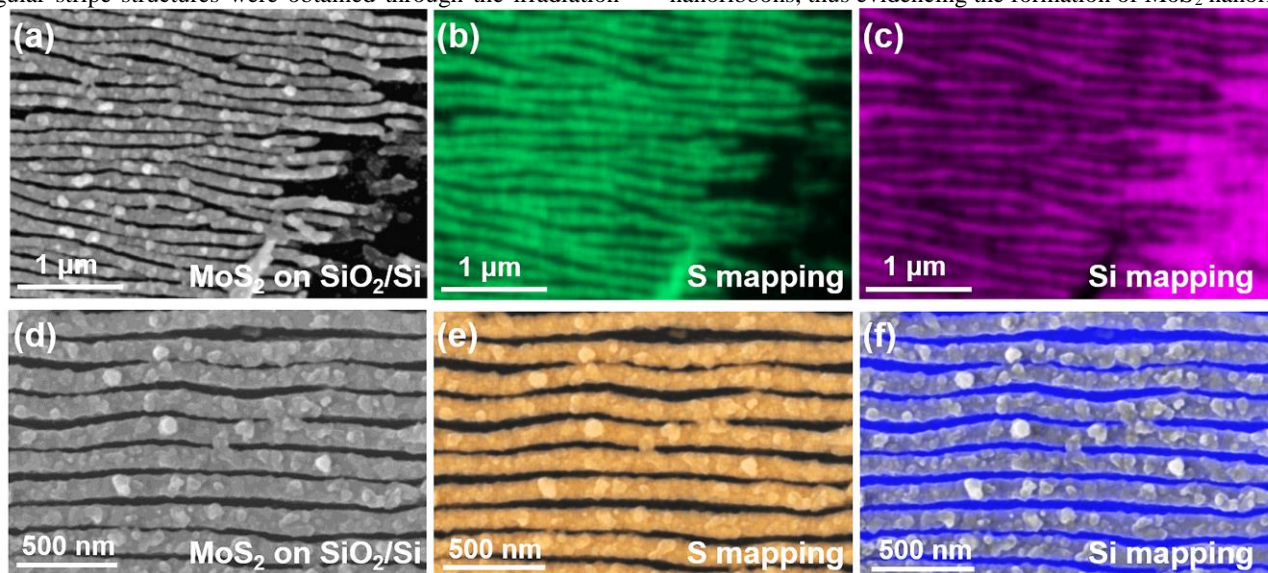

Figure 3 The formation of separated MoS$_2$ nanoribbons. (a) SEM image of the edge of a FLP-MoS$_2$ flake, and their (b) S and (c) Si EDX mapping images. (d) SEM image of MoS$_2$ nanoribbon arrays, and their (e) S and (f) Si EDX mapping images.

To investigate the change in chemical property of FLP-MoS$_2$ flaks, Raman and X-ray photoelectron spectroscopy (XPS) characterizations were conducted. Figure 4a and d show the Raman spectra of pristine MoS$_2$ and FLP-MoS$_2$. There was no Raman peak at 820 cm^{-1} originating from MoO$_3$, which indicted no formation of MoO$_3$ thus no obviously thermal oxidation for FLP-MoS$_2$ [44], due to the non-thermal effect of femtosecond laser processing [40]. No Raman peak of SiO$_2$ at 520 cm^{-1} was detected on pristine MoS$_2$ flake, however, there was an obviously Raman peak of SiO$_2$ was detected on FLP-MoS$_2$ flake, which indicated that substrate was also detected on FLP-MoS$_2$ flake [45, 46]. This result also proved the separation of MoS$_2$ nanoribbons and penetrating gaps between them, which was consistent with the results in Fig. 3. XPS Mo and O spectra of pristine MoS$_2$ and FLP-MoS$_2$ are also shown in Fig. 4 (XPS S spectra for them are shown in Fig. S1 and S2). The Mo 3d spectra for pristine MoS$_2$ is shown in Fig. 4b, which reveals three peaks at 227.2, 229.3, and 232.4 eV, respectively assigned to the S 2s orbital of divalent sulfur, and the Mo^{4+} 3d$_{5/2}$ and 3d$_{3/2}$ orbitals of tetravalent molybdenum. However, in Mo 3d spectra for FLP-MoS$_2$ (Fig. 4e), except the three peaks as shown in pristine MoS$_2$, there is a new peak at ~235 eV, which is assigned to the Mo^{6+} 3d$_{3/2}$ orbital of hexavalent molybdenum. The Mo^{6+} in FLP-MoS$_2$ was attributed to the Mo−O bonds formed through oxygen bonding to the unsaturated Mo bonds, defect sites, or edge of nanoribbons that generated from the damage and material removal of MoS$_2$ induced by femtosecond laser pulses [47, 48], Fig. 4c shows the O 1s spectra for pristine MoS$_2$, which reveals two peak at 532.6 and 533.4 eV, attributed to the divalent oxygen of

Si–O bonds and the nonvalent oxygen of oxygen molecules physically adsorbed on MoS$_2$ surface (O$_2$/MoS$_2$), respectively [49-51]. The divalent oxygen of Si–O bonds was derived from the 300-nm SiO$_2$/Si substrate, and oxygen molecules on MoS$_2$ surface should be attributed to the intrinsic defect and edge of the flake, which were active sites with physical adsorption capacity. However, in O 1s spectra for FLP-MoS$_2$ (Fig. 4f), except the strong and dominant peak assigned to divalent oxygen of Si–O bonds as shown in pristine MoS$_2$, it revealed stronger peak of nonvalent oxygen of O$_2$/MoS$_2$, indicating more oxygen molecules physically adsorbed on MoS$_2$ surface; it also revealed a new peak at approximately 530.5 eV assigned to the divalent oxygen of Mo–O

bonds [52, 53], which was consistent with the result of XPS Mo 3d spectra. These results indicated that more oxygen atoms/molecules were chemical and physical bonded to FLP-MoS$_2$. This can be attributed to the roughness defect-sites on MoS$_2$ nanoribbons and the long edges of these nanoribbons, for they contained numerous unsaturated edge sites and were numerous highly active centres, which can physically and chemically bonded with adsorbates such as O$_2$ molecules [54-56]. The oxygen absorption on MoS$_2$ not only led to the change in chemical valence of MoS$_2$, but also, according to previous reports, can lead p-type doping effect on MoS$_2$ with O$_2$ as electron acceptor and MoS$_2$ as electron donor [54].
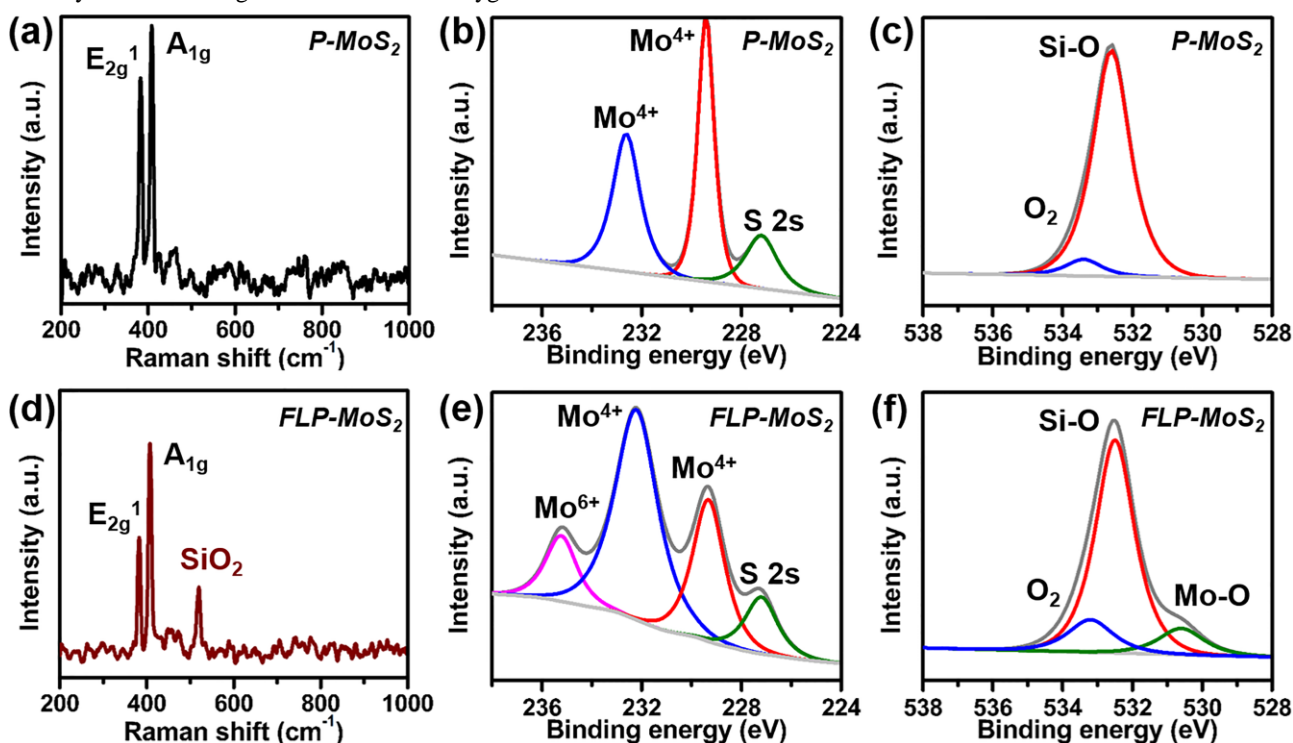
Figure 4 Raman and XPS spectra of P-MoS$_2$ and FLP-MoS$_2$. (a) Raman spectra of P-MoS$_2$. XPS peak-split results of (b) Mo 3d and (c) O 1s spectra of P-MoS$_2$. (d) Raman spectra of FLP-MoS$_2$. XPS peak-split results of (e) Mo 3d and (f) O 1s spectra of FLP-MoS$_2$.

To evaluate the electronic properties of prepared MoS$_2$ nanoribbon arrays, we fabricated a back gate FET by using MoS$_2$ nanoribbon arrays (NrA) on SiO2/p+ Si substrates as channel, with 5 nm Ti/ 75 nm Au as source and drain electrodes, through electron beam lithography (EBL), metal evaporation deposition, and a lift-off process. The electrical measurements of fabricated FET were performed by using a Keithley 4200 semiconductor characterization system in air and at room temperature. The schematic of the structure and measurement of the fabricated MoS$_2$ NrA-FET is shown in Fig. 5a. Figure 5b shows the SEM image of MoS$_2$ nanoribbon arrays used for fabricating the FET with channel length of $L \approx 3.4$ μm, integral channel width of $W \approx 6.6$ μm, ribbon number of about 38, and gate dielectric thickness of $d = 300$ nm. For comparison, pristine MoS$_2$ flake was also fabricated as a back-gated FET. Figure 5c shows the drain−source current (I_{DS}) versus drain−source voltage (V_{DS}) characteristics of this NrA-FET under different gate voltages (V_G) ranging from -15 to 15 V. For this output characteristic curve, the drain−source current changed linearly with the drain−source voltage, indicating nearly ohmic contact for this FET device. In addition, the output curve did not go through zero and exhibited a strong rectification of the drain−source current, which was different from the output characteristic curve of the FET fabricated by using

pristine/undamaged MoS$_2$ flake as shown in Fig. S3a. This may be attributed to the p-type chemical doping of oxygen molecules on MoS$_2$ nanoribbon arrays, which might cause transition of n-type channel to p-type channel or properties similar to pn junction [3].
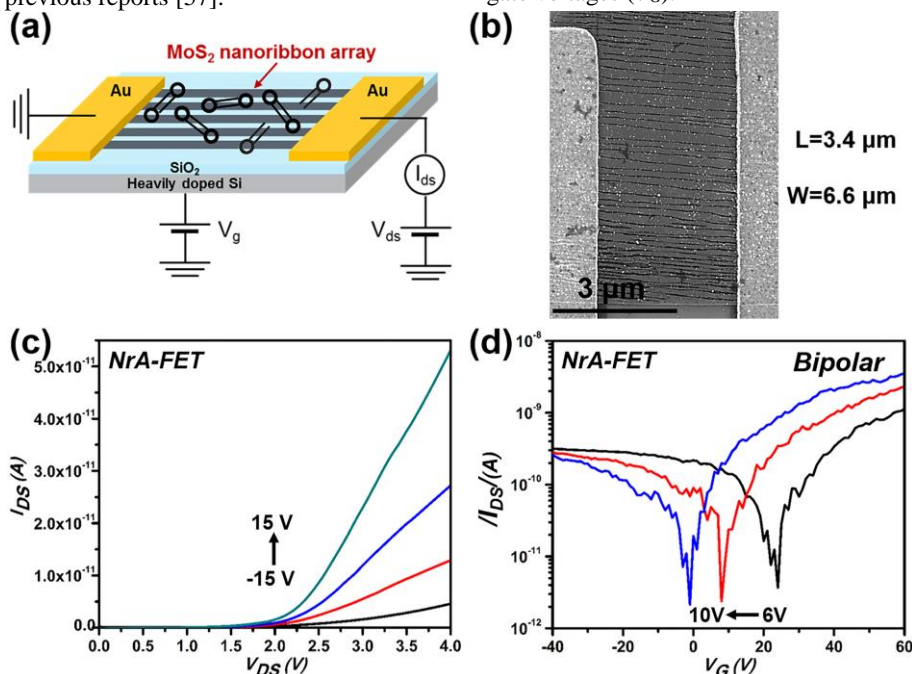
Figure 5d shows the drain−source current (I_{DS}) versus gate voltages (V_G) characteristics of this NrA-FET under different drain−source voltage (V_{DS}) ranging from 6 to 10 V. The trend of this transfer curve was non-monotone variation and exhibited a strong rectification of the drain−source current, which was different from the transfer characteristic curve of the FET fabricated by using pristine/undamaged MoS$_2$ flake. As shown in Fig. S3b, the transfer characteristic curve of pristine/undamaged MoS$_2$ FET exhibited n-type conduction. However, the transfer characteristic curve of MoS$_2$ NrA-FET exhibits bipolar conduction, similar to p-n type transfer conduction (Fig. 5d), with current chopping by a small voltage range. To further evaluate the electronic properties of this device, the on/off ratio, carrier mobility (μ), and subthreshold swing (SS) were calculated. The on/off ratio of the device was calculated to be 1.2×10^2 (p-type segment) and 1.7×10^3 (n-type segment) at the drain−source voltage (V_{DS}) of 10 V. The carrier mobility (μ) was calculated according to the following equation from previous reports [23],

$$\mu = \frac{L}{W} \frac{d}{\varepsilon_0 \varepsilon_r} \frac{1}{V_{DS}} \frac{\partial I_{DS}}{\partial V_G} \qquad (1)$$

where L and W are the length and width of FET channel, respectively; d, ε_0, and ε_r are the thickness, vacuum permittivity, and relative permittivity of grid dielectric layer, respectively; $\frac{\partial I_{DS}}{\partial V_G}$ can be calculated from the $I_{DS}-V_G$ curve. For this FET device, the length and width of channel were $L \approx 3.4$ μm and $W \approx 6.6$ μm; the grid dielectric layer was SiO$_2$, its thickness was $d \approx 300$ nm, and its vacuum permittivity and relative permittivity were $\varepsilon_0 \approx 8.85 \times 10^{-12}$ F/m and $\varepsilon_r \approx 3.9$ F/m [23], respectively. Hence, the carrier mobility of this device was calculated to be approximately 2.6×10^{-3} cm^2 V^{-1} s^{-1}. The SS was calculated according to the following equation from previous reports [57].

$$SS = \frac{\Delta V_G}{\Delta \log I_{DS}} \qquad (2)$$

And the SS of this device was calculated to be ~21 V/dec according to Eq. (2). The obvious strong rectification behavior of $I_{DS}-V_{DS}$ and $I_{DS}-V_G$ of the MoS$_2$ NrA-FET indicated the property change of material and the new device properties, which may enable new device applications. In addition, moderate surface modification of MoS$_2$ flakes by femtosecond laser pulses would also tune the n-type electronic properties of MoS$_2$ FET: as shown in Fig. S3, the on/off ratio of MoS$_2$ FET was increased by two magnitude; as shown in Fig. S4, the drain−source current (I_{DS}) increased quicker and reached saturation faster with the increase of gate voltages (V_G).

Figure 5 Electrical test of MoS$_2$ NrA-FET. a) Schematic of the structure and measurement of fabricated MoS$_2$ NrA-FET. b) SEM image of MoS$_2$ nanoribbon arrays used for fabricating FET. c) Output and d) transfer characteristic curve of the fabricated MoS$_2$ NrA-FET.

3 Conclusions

Femtosecond laser pulse direct writing was used to nonthermally modify multilayer MoS$_2$ flakes, induce separated MoS$_2$ nanoribbon arrays, and arbitrarily pattern MoS$_2$ flakes to form different MoS$_2$ micro/nanostructures. Optical microscope, AFM, and SEM were performed to characterize the physical micromorphology of laser processed-MoS$_2$ flakes. EDX mapping indicated the separation of MoS$_2$ nanoribbons, proving the formation of MoS$_2$ nanoribbons rather than surface structures on MoS$_2$. Raman spectra indicated the non-thermal effect of femtosecond laser processing, also proved the separation of MoS$_2$ nanoribbons and the penetrating gaps between them. XPS spectra indicated that more oxygen molecules were chemical and physical bonded to FLP-MoS$_2$, which attributed to the roughness defect sites on MoS$_2$ nanoribbons and the long edges of the nanoribbons that contained numerous unsaturated edge sites and highly active centres. A MoS$_2$ NrA-FET was fabricated and electrical tests were conducted to evaluate the electronic properties of prepared MoS$_2$ nanoribbon arrays. Results indicated that the output and transfer characteristic curves exhibited strong rectification (not going through zero and bipolar conduction) of drain−source current, which were different from that of FET fabricated by using pristine/undamaged MoS$_2$ flake.

This may be attributed the coordinate structures and p-type chemical doping of oxygen molecules on MoS$_2$ nanoribbon arrays, which might cause transition of n-type channel to p-type channel or properties similar to pn junction. At last, the on/off ratio, carrier mobility, and SS were also calculated. The proposed method indicated the ability of femtosecond laser pulses to directly induce two-dimension nanostructures, property change in material, and new device properties, which may future enable new device applications.

4 Experimental

4.1 Femtosecond laser pulse processing

The light path setup of our femtosecond laser pulse processing system was reported in our previous study [8].

4.2 Characterization of MoS$_2$ nanostructures

The optical images were obtained using an Olympus microscope. The AFM characterization was carried out using a SPM-960 AFM. The SEM images and EDX mapping spectra were obtained using a Hitachi scanning electron microscope. Raman spectra were obtained using a Renishaw InVia Reflex spectrometer (532 nm light source). XPS was performed using a PHI Quantera X-ray photoelectron spectrometer.

4.3 Device fabrication and electrical characterization

Multilayer MoS_2 flakes were placed on p+Si/SiO$_2$ (300 nm) substrates and processed by femtosecond laser pulse. Then the substrates were spin-coated with poly methyl methacrylate (PMMA) solution. The source and drain electrodes were fabricated through three main steps: standard electron-beam lithography (EBL) was performed by Zeiss Supra55 SEM and Raith pattern generator to pattern the PMMA masks; 5 nm Ti/75 nm Au were deposited through electronic beam evaporation; a lift-off process was performed in acetone. The electrical measurements of the fabricated MoS_2 FET were performed by using a Keithley 4200 semiconductor characterization system in air and at room temperature.

Acknowledgements

Electronic Supplementary Material: Supplementary material (Supplementary XPS Mo, O, and S spectra of pristine MoS_2, XPS S spectra of FLP-MoS_2, and supplementary electrical test results of MoS_2 FETs with moderate surface modification by femtosecond laser pulses) is available in the online version of this article at http://dx.doi.org/10.1007/s12274-***-****-* (automatically inserted by the publisher).

References

[1] Chhowalla, M.; Jena, D.; Zhang, H. Two-dimensional semiconductors for transistors. *Nat. Rev. Mater.* **2016,** *1*, 16052.

[2] Bertolazzi, S.; Bonacchi, S.; Nan, G.; Pershin, A.; Beljonne, D.; Samorì, P. Engineering chemically active defects in monolayer MoS_2 transistors via ion-beam irradiation and their healing via vapor deposition of alkanethiols. *Adv. Mater.* **2017,** *29*, 1606760.

[3] Nam, H.; Wi, S.; Rokni, H.; Chen, M.; Priessnitz, G.; Lu, W.; Liang, X. MoS_2 transistors fabricated via plasma-assisted nanoprinting of few-layer MoS_2 flakes into large-area arrays. *ACS Nano* **2013,** *7*, 5870-5881.

[4] Eda, G.; Maier, S. A. Two-dimensional crystals: Managing light for optoelectronics. *ACS Nano* **2013,** *7*, 5660-5665.

[5] Mak, K. F.; He, K.; Lee, C.; Lee, G. H.; Hone, J.; Heinz, T. F.; Shan, J. Tightly bound trions in monolayer MoS_2. *Nat. Mater.* **2013,** *12*, 207-211.

[6] Yu, Y.; Ji, Z.; Zu, S.; Du, B.; Kang, Y.; Li, Z.; Zhou, Z.; Shi, K.; Fang, Z. Ultrafast plasmonic hot electron transfer in au nanoantenna/MoS_2 heterostructures. *Adv. Funct. Mater.* **2016,** *26*, 6394-6401.

[7] Behura, S.; Berry, V. Interfacial nondegenerate doping of MoS_2 and other two-dimensional semiconductors. *ACS Nano* **2015,** *9*, 2227-2230.

[8] Zuo, P.; Jiang, L.; Li, X.; Li, B.; Ran, P.; Li, X.; Qu, L.; Lu, Y. Metal (Ag, Pt)–MoS_2 hybrids greenly prepared through photochemical reduction of femtosecond laser pulses for sers and her. *ACS Sustain. Chem. Eng.* **2018,** *6*, 7704-7714.

[9] Lu, J.; Liu, H.; Tok, E. S.; Sow, C.-H. Interactions between lasers and two-dimensional transition metal dichalcogenides. *Chem. Soc. Rev.* **2016,** *45*, 2494-2515.

[10] Cho, K.; Pak, J.; Kim, J.-K.; Kang, K.; Kim, T.-Y.; Shin, J.; Choi, B. Y.; Chung, S.; Lee, T. Contact-engineered electrical properties of MoS_2 field-effect transistors via selectively deposited thiol-molecules. *Adv. Mater.* **2018,** *30*, 1705540.

[11] Cheng, R.; Jiang, S.; Chen, Y.; Liu, Y.; Weiss, N.; Cheng, H.-C.; Wu, H.; Huang, Y.; Duan, X. Few-layer molybdenum disulfide transistors and circuits for high-speed flexible electronics. *Nat. Commun.* **2014,** *5*, 5143.

[12] Gao, G.; Wan, B.; Liu, X.; Sun, Q.; Yang, X.; Wang, L.; Pan, C.; Wang, Z. L. Tunable tribotronic dual-gate logic devices based on 2D MoS_2 and

black phosphorus. *Adv. Mater.* **2018,** *30*, 1705088.

[13] Yoo, H.; Hong, S.; On, S.; Ahn, H.; Lee, H.-K.; Hong, Y. K.; Kim, S.; Kim, J.-J. Chemical doping effects in multilayer MoS_2 and its application in complementary inverter. *ACS Appl. Mater. Inter.* **2018,** *10*, 23270-23276.

[14] Pak, Y.; Park, W.; Mitra, S.; Sasikala Devi, A. A.; Loganathan, K.; Kumaresan, Y.; Kim, Y.; Cho, B.; Jung, G.-Y.; Hussain, M. M. et al. Enhanced performance of MoS_2 photodetectors by inserting an ald-processed TiO_2 interlayer. *Small* **2018,** *14*, 1703176.

[15] Woo, Y.; Hong, W.; Yang, S. Y.; Kim, H. J.; Cha, J.-H.; Lee, J. E.; Lee, K. J.; Kang, T.; Choi, S.-Y. Large-area CVD-grown MoS_2 driver circuit array for flexible organic light-emitting diode display. *Adv. Electron. Mater.* **2018,** *0*, 1800251.

[16] Choi, M.; Park, Y. J.; Sharma, B. K.; Bae, S.-R.; Kim, S. Y.; Ahn, J.-H. Flexible active-matrix organic light-emitting diode display enabled by MoS_2 thin-film transistor. *Sci. Adv.* **2018,** *4*.

[17] Zhang, J.; Lang, X. Y.; Zhu, Y. F.; Jiang, Q. Strain tuned InSe/MoS_2 bilayer van der waals heterostructures for photovoltaics or photocatalysis. *Phys. Chem. Chem. Phys.* **2018,** *20*, 17574-17582.

[18] Xu, M.; Chen, Y.; Xiong, F.; Wang, J.; Liu, Y.; Lv, J.; Li, Y.; Wang, Y.; Chen, Z.; Ma, Y. A hidden symmetry-broken phase of MoS_2 revealed as a superior photovoltaic material. *J. Mater. Chem. A* **2018,** *6*, 16087-16093.

[19] Chen, Q.; Lu, J.; Liang, L.; Zheliuk, O.; Ali El Yumin, A.; Ye, J. Continuous low-bias switching of superconductivity in a MoS_2 transistor. *Adv. Mater.* **2018,** *30*, 1800399.

[20] Saito, Y.; Nakamura, Y.; Bahramy, M. S.; Kohama, Y.; Ye, J.; Kasahara, Y.; Nakagawa, Y.; Onga, M.; Tokunaga, M.; Nojima, T. et al. Superconductivity protected by spin–valley locking in ion-gated MoS_2. *Nat. Phys.* **2015,** *12*, 144.

[21] Kumar, R.; Goel, N.; Kumar, M. UV-activated MoS_2 based fast and reversible NO_2 sensor at room temperature. *ACS Sensors* **2017,** *2*, 1744-1752.

[22] Ryu, B.; Nam, H.; Oh, B.-R.; Song, Y.; Chen, P.; Park, Y.; Wan, W.; Kurabayashi, K.; Liang, X. Cyclewise operation of printed MoS_2 transistor biosensors for rapid biomolecule quantification at femtomolar levels. *ACS Sensors* **2017,** *2*, 274-281.

[23] Zhao, J.; Yu, H.; Chen, W.; Yang, R.; Zhu, J.; Liao, M.; Shi, D.; Zhang, G. Patterned peeling 2D MoS_2 off the substrate. *ACS Appl. Mater. Inter.* **2016,** *8*, 16546-16550.

[24] Huang, M.; Li, S.; Zhang, Z.; Xiong, X.; Li, X.; Wu, Y. Multifunctional high-performance van der waals heterostructures. *Nat. Nanotechnol.* **2017,** *12*, 1148.

[25] Radisavljevic, B.; Radenovic, A.; Brivio, J.; Giacometti, V.; Kis, A. Single-layer MoS_2 transistors. *Nat. Nanotechnol.* **2011,** *6*, 147.

[26] Cong, R.; Qiao, S.; Liu, J.; Mi, J.; Yu, W.; Liang, B.; Fu, G.; Pan, C.; Wang, S. Ultrahigh, ultrafast, and self-powered visible-near-infrared optical position-sensitive detector based on a CVD-prepared vertically standing few-layer MoS_2/Si heterojunction. *Adv. Sci.* **2018,** *5*, 1700502.

[27] Liu, H.; Zhu, Y.; Meng, Q.; Lu, X.; Kong, S.; Huang, Z.; Jiang, P.; Bao, X. Role of the carrier gas flow rate in monolayer MoS_2 growth by modified chemical vapor deposition. *Nano Res.* **2017,** *10*, 643-651.

[28] Liu, K.-K.; Zhang, W.; Lee, Y.-H.; Lin, Y.-C.; Chang, M.-T.; Su, C.-Y.; Chang, C.-S.; Li, H.; Shi, Y.; Zhang, H. et al. Growth of large-area and highly crystalline MoS_2 thin layers on insulating substrates. *Nano Lett.* **2012,** *12*, 1538-1544.

[29] Pak, S.; Lee, J.; Lee, Y.-W.; Jang, A. R.; Ahn, S.; Ma, K. Y.; Cho, Y.; Hong, J.; Lee, S.; Jeong, H. Y. et al. Strain-mediated interlayer coupling effects on the excitonic behaviors in an epitaxially grown MoS_2/WS$_2$ van der waals heterobilayer. *Nano Lett.* **2017,** *17*, 5634-5640.

[30] Shi, Y.; Zhou, W.; Lu, A.-Y.; Fang, W.; Lee, Y.-H.; Hsu, A. L.; Kim, S. M.; Kim, K. K.; Yang, H. Y.; Li, L.-J. et al. Van der waals epitaxy of MoS_2 layers using graphene as growth templates. *Nano Lett.* **2012,** *12*, 2784-2791.

[31] Xue, Y.; Zhang, Y.; Liu, Y.; Liu, H.; Song, J.; Sophia, J.; Liu, J.; Xu, Z.; Xu, Q.; Wang, Z. et al. Scalable production of a few-layer MoS_2/WS$_2$ vertical heterojunction array and its application for photodetectors. *ACS Nano* **2016,** *10*, 573-580.

[32] Choudhary, N.; Park, J.; Hwang, J. Y.; Chung, H.-S.; Dumas, K. H.; Khondaker, S. I.; Choi, W.; Jung, Y. Centimeter scale patterned growth of vertically stacked few layer only 2D MoS₂/WS₂ van der waals heterostructure. *Sci. Rep.* **2016,** *6*, 25456.

[33] Chen, X.; Park, Y. J.; Das, T.; Jang, H.; Lee, J.-B.; Ahn, J.-H. Lithography-free plasma-induced patterned growth of MoS₂ and its heterojunction with graphene. *Nanoscale* **2016,** *8*, 15181-15188.

[34] Kim, H.-J.; Kim, H.; Yang, S.; Kwon, J.-Y. Grains in selectively grown MoS₂ thin films. *Small* **2017,** *13*, 1702256.

[35] Han, G. G. D.; Tu, K.-H.; Niroui, F.; Xu, W.; Zhou, S.; Wang, X.; Bulović, V.; Ross, C. A.; Warner, J. H.; Grossman, J. C. Photoluminescent arrays of nanopatterned monolayer MoS₂. *Adv. Funct. Mater.* **2017,** *27*, 1703688.

[36] Jung, Y.; Shen, J.; Liu, Y.; Woods, J. M.; Sun, Y.; Cha, J. J. Metal seed layer thickness-induced transition from vertical to horizontal growth of MoS₂ and WS₂. *Nano Lett.* **2014,** *14*, 6842-6849.

[37] Mahjouri-Samani, M.; Lin, M.-W.; Wang, K.; Lupini, A. R.; Lee, J.; Basile, L.; Boulesbaa, A.; Rouleau, C. M.; Puretzky, A. A.; Ivanov, I. N. et al. Patterned arrays of lateral heterojunctions within monolayer two-dimensional semiconductors. *Nat. Commun.* **2015,** *6*, 7749.

[38] Cao, L.; Yang, S.; Gao, W.; Liu, Z.; Gong, Y.; Ma, L.; Shi, G.; Lei, S.; Zhang, Y.; Zhang, S. et al. Direct laser-patterned micro-supercapacitors from paintable MoS₂ films. *Small* **2013,** *9*, 2905-2910.

[39] Lu, J.; Lu, J. H.; Liu, H.; Liu, B.; Chan, K. X.; Lin, J.; Chen, W.; Loh, K. P.; Sow, C. H. Improved photoelectrical properties of MoS₂ films after laser micromachining. *ACS Nano* **2014,** *8*, 6334-6343.

[40] Jiang, L.; Wang, A.-D.; Li, B.; Cui, T.-H.; Lu, Y.-F. Electrons dynamics control by shaping femtosecond laser pulses in micro/nanofabrication: Modeling, method, measurement and application. *Light: Sci. Appl.* **2018,** *7*, 17134.

[41] Huang, M.; Zhao, F.; Cheng, Y.; Xu, N.; Xu, Z. Origin of laser-induced near-subwavelength ripples: Interference between surface plasmons and incident laser. *ACS Nano* **2009,** *3*, 4062-4070.

[42] Shuangshuang, H.; Yanyan, H.; Pingxin, X.; Yi, Z.; Shian, Z.; Tianqing, J.; Zhenrong, S.; Jianrong, Q.; Zhizhan, X. Formation of long- and short-periodic nanoripples on stainless steel irradiated by femtosecond laser pulses. *J. Phys. D: Appl. Phys.* **2011,** *44*, 505401.

[43] Xia, B.; Jiang, L.; Li, X.; Yan, X.; Zhao, W.; Lu, Y. High aspect ratio, high-quality microholes in pmma: A comparison between femtosecond laser drilling in air and in vacuum. *Appl. Phys. A* **2015,** *119*, 61-68.

[44] Paradisanos, I.; Kymakis, E.; Fotakis, C.; Kioseoglou, G.; Stratakis, E. Intense femtosecond photoexcitation of bulk and monolayer MoS₂. *Appl. Phys. Lett.* **2014,** *105*, 041108.

[45] Serincan, U.; Kartopu, G.; Guennes, A.; Finstad, T. G.; Turan, R.; Ekinci, Y.; Bayliss, S. C. Characterization of ge nanocrystals embedded in SiO₂ by raman spectroscopy. *Semicond. Sci. Tech.* **2004,** *19*, 247.

[46] Nesheva, D.; Raptis, C.; Perakis, A. Raman scattering and photoluminescence from si nanoparticles in annealed SiOₓ thin films. *J. Appl. Phys.* **2002,** *92*, 4678-4683.

[47] Wei, X.; Yu, Z.; Hu, F.; Cheng, Y.; Yu, L.; Wang, X.; Xiao, M.; Wang, J.; Wang, X.; Shi, Y. Mo-o bond doping and related-defect assisted enhancement of photoluminescence in monolayer MoS₂. *AIP Adv.* **2014,** *4*, 123004.

[48] da Silveira Firmiano, E. G.; Rabelo, A. C.; Dalmaschio, C. J.; Pinheiro, A. N.; Pereira, E. C.; Schreiner, W. H.; Leite, E. R. Supercapacitor electrodes obtained by directly bonding 2D MoS₂ on reduced graphene oxide. *Adv. Energy Mater.* **2014,** *4*.

[49] Hollinger, G. Structures chimique et electronique de l'interface SiO₂-Si. *Applications. Surf. Sci.* **1981,** *8*, 318-336.

[50] Shuxian, Z.; Hall, W. K.; Ertl, G.; Knözinger, H. X-ray photoemission study of oxygen and nitric oxide adsorption on MoS₂. *J. of Catal.* **1986,** *100*, 167-175.

[51] Finster, J.; Klinkenberg, E.-D.; Heeg, J.; Braun, W. Esca and sexafs investigations of insulating materials for ulsi microelectronics. *Vacuum* **1990,** *41*, 1586-1589.

[52] Colton, R. J.; Guzman, A. M.; Rabalais, J. W. Electrochromism in some thin‐film transition‐metal oxides characterized by x‐ray electron spectroscopy. *J. Appl. Phys.* **1978,** *49*, 409-416.

[53] Chowdari, B.; Tan, K.; Chia, W.; Gopalakrishnan, R. X-ray photoelectron spectroscopic studies of molybdenum phosphate glassy system. *J. Non-cryst. Solids* **1990,** *119*, 95-102.

[54] Nan, H.; Wang, Z.; Wang, W.; Liang, Z.; Lu, Y.; Chen, Q.; He, D.; Tan, P.; Miao, F.; Wang, X. et al. Strong photoluminescence enhancement of MoS₂ through defect engineering and oxygen bonding. *ACS Nano* **2014,** *8*, 5738-5745.

[55] Zhou, W.; Zou, X.; Najmaei, S.; Liu, Z.; Shi, Y.; Kong, J.; Lou, J.; Ajayan, P. M.; Yakobson, B. I.; Idrobo, J.-C. Intrinsic structural defects in monolayer molybdenum disulfide. *Nano Lett.* **2013,** *13*, 2615-2622.

[56] Yan, Y.; Xia, B.; Ge, X.; Liu, Z.; Wang, J.-Y.; Wang, X. Ultrathin MoS₂ nanoplates with rich active sites as highly efficient catalyst for hydrogen evolution. *ACS Appl. Mater. Inter.* **2013,** *5*, 12794-12798.

[57] Wang, X.; Zhang, T.-B.; Yang, W.; Zhu, H.; Chen, L.; Sun, Q.-Q.; Zhang, D. W. Improved integration of ultra-thin high-k dielectrics in few-layer MoS₂ FET by remote forming gas plasma pretreatment. *Appl. Phys. Lett.* **2017,** *110*, 053110.

1
2
3
4
5
6
7
8
9
10
11
12
13
14
15
16
17
18
19
20
21
22
23
24
25
26
27
28
29
30
31
32
33
34
35
36
37
38
39
40
41
42
43
44
45
46
47
48
49
50
51
52
53
54
55
56
57
58
59
60
61
62
63
64
65

Electronic Supplementary Material

Maskless micro/nanopatterning and bipolar electrical-rectification of MoS₂ flakes through femtosecond laser direct writing

Pei Zuo[1], Lan Jiang[1], Xin Li[1] (✉), Mengyao Tian[1], Chenyang Xu[1], Yongjiu Yuan[1], Peng Ran[1], Bo Li[1], Yongfeng Lu[2]

[1] *Laser Micro/Nano Fabrication Lab, School of Mechanical Engineering, Beijing Institute of Technology, Beijing 100081, China*
[2] *Laser Assisted Nano Engineering Lab, Department of Electrical Engineering, University of Nebraska-Lincoln, Lincoln, NE 68588-0511, USA*
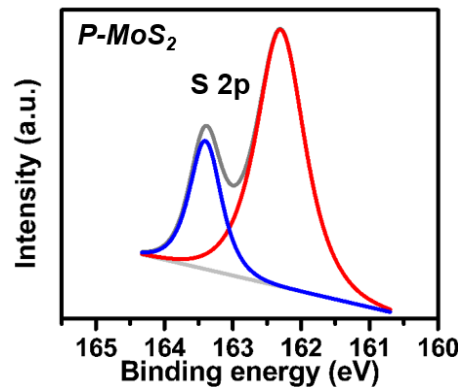
Supplementary figures and analysis.

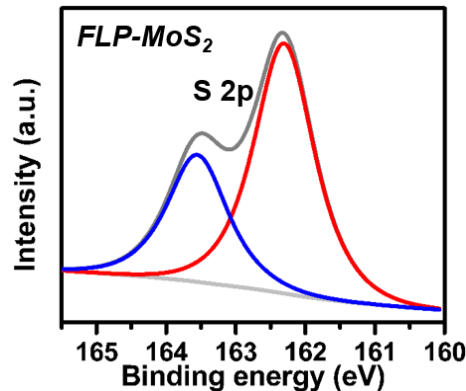**Figure S1** XPS peak-split results of S 2p spectra of P-MoS₂.

Figure S2 XPS peak-split results of S 2p spectra of FLP-MoS₂.

Surface moderate modification of MoS₂ flakes through femtosecond laser pulse processing for FET (-1 and -2). Figure S3 and S4 show the electrical test results for two MoS₂ FET, which are MoS₂ FET-1 and MoS₂ FET-2, before and after surface modified.

Figure S3a and c show the drain−source current (I_{DS}) versus drain−source voltage (V_{DS}) characteristics of MoS₂ FET-1 before and after surface moderate modification under different gate voltages (V_G) ranging from -10 to 10 V. For these output characteristic curve, the drain−source current changed linearly with the drain−source voltage, indicating nearly ohmic contact for these FET device. Figure S3b and d show the drain−source current (I_{DS}) versus gate voltages (V_G) characteristics of MoS₂ FET-1 before and after surface moderate modification under different drain−source voltage (V_{DS}) ranging from 0.05 to 0.5 V. These transfer characteristic curve of pristine/undamaged and surface moderate modified MoS₂ FET exhibited n-type conduction. To further compare the change in electronic properties of this device, the on/off ratio, carrier mobility (μ), and subthreshold swing (SS) were calculated. For pristine/undamaged MoS₂ FET-1, the on/off ratio, carrier mobility (μ), and SS were respectively 2.84×10^3, 13.87 cm² V⁻¹ s⁻¹, and 14.3 V/dec; for surface modified MoS₂ FET-1, the on/off ratio, carrier mobility (μ), and SS were respectively 1.85×10^5, 1.55 cm² V⁻¹ s⁻¹, and 9.4 V/dec. These results indicated that after femtosecond laser modification processed, the on/off ratio of MoS₂ FET-1 was increased by two magnitude, whereas the carrier mobility was decreased. The increase of on/off ratio might be attributed to the thinning effect of femtosecond laser on MoS₂ flake [S1]. And the decrease of carrier mobility might be attributed to the defect states on laser modified-MoS₂, which can reduce the portion of mobile carriers in conduction band and increase the portion of trapped carriers that do not contribute to charge transport, hence leading to

Address correspondence to Xin Li, lixin02@bit.edu.cn

the degradation of effective mobility [S2].
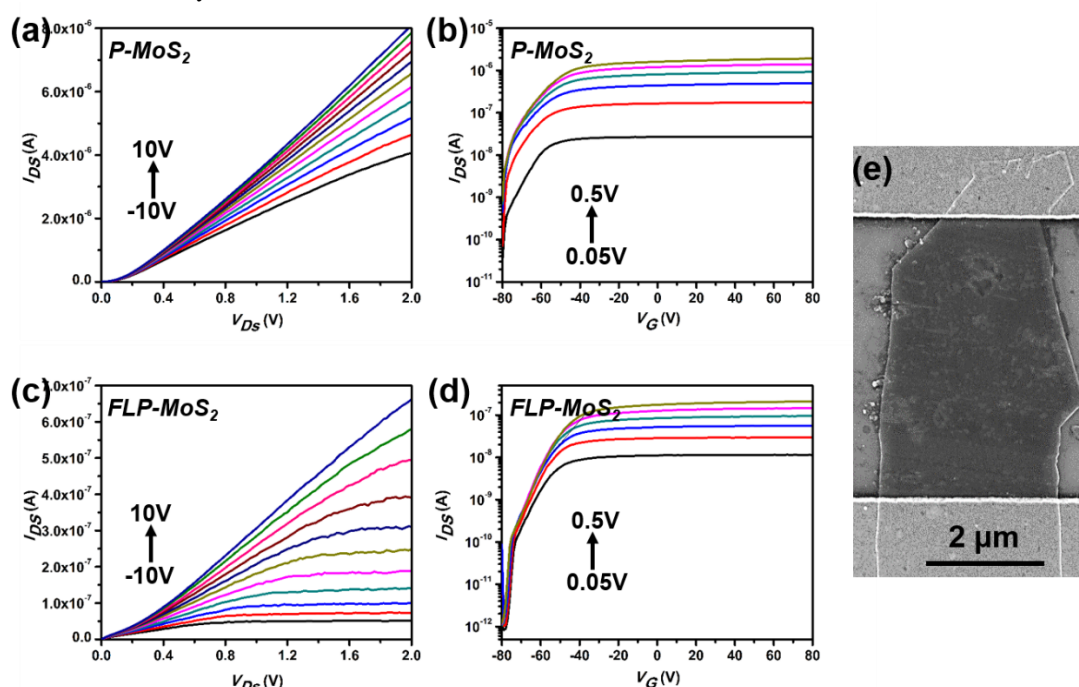
Figure S3 Electrical test of MoS$_2$ FET-1 before and after surface modification. (a) Output and (b) transfer characteristic curve of MoS$_2$ FET-1 before surface modification. (c) Output and (d) transfer characteristic curve of MoS$_2$ FET-1 after surface modification. (e) SEM image of MoS$_2$ FET-1 after surface modification.

Figure S4a and c show the drain−source current (I_{DS}) versus drain−source voltage (V_{DS}) characteristics of MoS$_2$ FET-2 before and after surface moderate modification under different gate voltages (V_G) ranging from -10 to 10 V. For these output characteristic curve, the drain−source current changed linearly with the drain−source voltage, indicating nearly ohmic contact for these FET device. Figure S4b and d show the drain−source current (I_{DS}) versus gate voltages (V_G) characteristics of MoS$_2$ FET-2 before and after surface moderate modification under different drain−source voltage (V_{DS}) ranging from 0.75 to 1.5 V. These transfer characteristic curve of pristine/undamaged and surface moderate modified MoS$_2$ FET exhibited n-type conduction. To further compare the change of electronic properties of this device, the on/off ratio, carrier mobility (μ), and subthreshold swing (SS) were calculated. For pristine/undamaged and surface modified MoS$_2$ FET-2, the on/off ratio and carrier mobility (μ) were no changed, which were respectively 1.13×10^5 and 3.5×10^{-2} cm^2 V^{-1} s^{-1}, and SS were 18.5 and 11.7 V/dec, respectively. However, the drain−source current (I_{DS}) of surface modified MoS$_2$ FET-2 increased quicker and reached saturation faster with the increase of gate voltages (V_G) compared with that of pristine/undamaged MoS$_2$ FET-2.
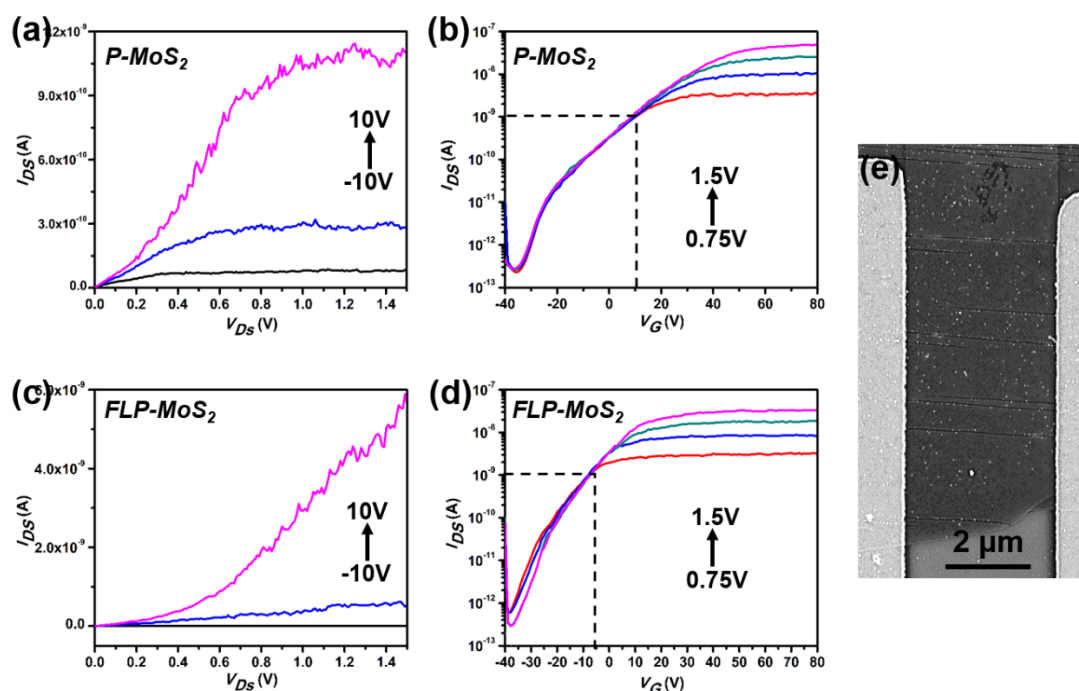
Figure S4 Electrical test of MoS$_2$ FET-2 before and after surface modification. (a) Output and (b) transfer characteristic curve of MoS$_2$ FET-2 before surface modification. (c) Output and (d) transfer characteristic curve of MoS$_2$ FET-2 after surface modification. (e) SEM image of MoS$_2$ FET-2 after surface modification.

Reference

[S1]   Chen, M.; Nam, H.; Wi, S.; Ji, L.; Ren, X.; Bian, L.; Lu, S.; Liang, X. Stable few-layer MoS$_2$ rectifying diodes formed by plasma-assisted doping. *Appl. Phys. Lett.* **2013,** *103*, 142110.

[S2]   Bertolazzi, S.; Bonacchi, S.; Nan, G.; Pershin, A.; Beljonne, D.; Samorì, P. Engineering chemically active defects in monolayer MoS$_2$ transistors via ion-beam irradiation and their healing via vapor deposition of alkanethiols. *Adv. Mater.* **2017,** *29*, 1606760.